Modeling of multicomponent-fuel drop-laden mixing layers having a multitude of species

P. C. Le Clercq and J. Bellan
Jet Propulsion Laboratory, California Institute of Technology

November 20, 2003

Corresponding Author:
Josette Bellan
Jet Propulsion Laboratory
California Institute of Technology
4800 Oak Grove Drive
M/S 125-109
Pasadena CA 91109-8099 USA
Tel: (818)354-6959, Fax: (818)393-5011
e-mail: Josette.Bellan@jpl.nasa.gov
Submitted to 30th International Symposium on Combustion
Colloquium on Heterogeneous Combustion (Sprays)
Short Title: Multicomponent-fuel drop-laden mixing layers
Keywords: multicomponent fuel sprays

Abstract

A formulation representing multicomponent-fuel (MC-fuel) composition as a Probability Distribution Function (PDF) depending on the molar weight is used to construct a model of a large number of MC-fuel drops evaporating in a gas flow, so as to assess the extent of fuel specificity on the vapor composition. The PDF is a combination of two Gamma PDFs, which was previously shown to duplicate the behavior of a fuel composed of many species during single drop evaporation. The conservation equations are Eulerian for the flow and Lagrangian for the physical drops, all of which are individually followed. The gas conservation equations for mass, momentum, species and energy, are complemented by differential conservation equations for the first four moments of the gas-composition PDF; all coupled to the perfect gas equation of state. Source terms in all conservation equations couple the gas phase to the drops. The drop conservation equations for mass, position, momentum and energy are complemented by differential equations for four moments of the liquid-composition PDF. The simulations are performed for a three-dimensional mixing layer whose lower stream is initially laden with drops. Initial perturbations excite the layer to promote the double pairing of its four initial spanwise vortices to an ultimate vortex. The drop temperature is initially lower than that of the surrounding gas, initiating drop heating and evaporation. The results focus on both evolution and the state of the drops and gas when layers reach a momentum-thickness maximum past the double vortex pairing; particular emphasis is on the gas composition. Comparisons between simulations with n-decane, diesel and three kerosenes show that at same initial Reynolds number and Stokes number distribution, a single-component fuel cannot represent MC fuels. Substantial differences among the MC-fuel vapor composition indicates that fuel specificity must be captured for the prediction of combustion.

1 Introduction

The overwhelming majority of fuels used in spray combustion devices are complex mixtures of a myriad of chemical species; examples are diesel, gasoline and kerosene. The traditional way of modeling these fuels has been to consider the mixture as the sum of all its individual species [1] [2] or as the sum of a solvent and a solute [3]; for obvious reasons, we call this the 'discrete' species approach (DSA). Complex fuels have so far not been simulated using the DSA, due to computational overhead associated with a large number of species. Ascertaining the role of different species is, however, important during combustion because they have different impacts depending on the application. Recent developments in the modeling of multicomponent (MC) fuel drops have opened intriguing possibilities for modeling MC-fuel sprays [4] [5] [6], [7]. These recent models are based on the well-established theory of Continuous Thermodynamics (CT) [8] [9] in which the chemical potential for a mixture containing numerous components is appropriately represented, and the Gibbs function is derived through molecular thermodynamic methods in terms of the probability distribution function (PDF) describing the mixture composition. The concepts are fundamental and independent of the physicochemical model chosen for the chemical potential. Having specified an initial PDF, the evolution of the mixture is governed by thermodynamic relationships and/or conservation equations. Although the most general PDF will depend on many variables, it has been shown, with validation, that the single-Gamma PDF depending on the molar weight, m, can represent a homologous species class [9]- [12].

Single-Gamma PDF models applied to drop evaporation [4] [5] [6] are, however, restricted to negligible fuel vapor in the drop-surrounding gas, as shown by Harstad et al. [7]. A combination of two Gamma PDFs (DGPDF) as a function of m is necessary to capture the evaporation of drops in a gas containing substantial fuel vapor [7], as in sprays. Moreover, Harstad and Bellan [13] have enlarged the DGPDF concept through appropriate thermodynamic modeling and shown that a single DGPDF can represent several homologous species classes.

This study addresses the problem of MC-fuel drop evaporation in shear flows, such as in sprays, and inquires into the species distribution in a pre-transitional flow. The interest is here on simulating situations where the drop evaporation, while still being relatively slow compared to that during combustion, is larger than in the SGPDF study, with the gas phase which may contain substantial vapor that could condense on the drops. The focus is on studying the influence of the fuel type and the freestream gas temperature in determining the layer-fuel composition.

2 Conservation equations

The equations follow in concept the single-component (SC) study of Miller and Bellan [14] and emulate the SC investigation of Okong'o and Bellan [15], in that the gas phase is described in an Eulerian frame and the drops are followed in a Lagrangian frame. The drops are assumed much smaller than the Kolmogorov scale, meaning that they can be treated as sources of mass, species, momentum and energy for the gas [16] [17]. The MC-fuel composition is described by

$$P(m;\alpha_1,\beta_1,\alpha_2,\beta_2,\epsilon) = (1-\epsilon)f_\Gamma^{(1)} + \epsilon f_\Gamma^{(2)}, \quad (1)$$

where $f_\Gamma^{(k)} = f_\Gamma(m;\alpha_k,\beta_k)$ with $k \in [1,2]$, ϵ is a weighting parameter ($0 \leqslant \epsilon \leqslant 1$), $\int_\gamma^\infty P(m)dm = 1$ and

$$f_\Gamma(m) = \frac{(m-\gamma)^{\alpha-1}}{\beta^\alpha \Gamma(\alpha)} \exp\left[-\left(\frac{m-\gamma}{\beta}\right)\right] \quad (2)$$

where $\Gamma(\alpha)$ is the Gamma function. The origin of f is specified by γ, and its shape is determined by α and β. Thus, $P(m;\alpha_1,\beta_1,\alpha_2,\beta_2,\epsilon)$ is determined at each time t by the vector $\boldsymbol{\eta} \equiv (\alpha_1,\beta_1,\alpha_2,\beta_2,\epsilon)$; $\gamma_1 = \gamma_2 = \gamma$ is assumed. Harstad et al. [7] have shown that P can be determined by an inverse mapping from its first four moments, θ, ψ, ξ_3 and ξ_4, with a fifth parameter empirically calculated. Thus, at each t, P_l describes the liquid-fuel composition (subscript l denotes the liquid), being drop specific; P_v describes the vapor composition (subscript v denotes the vapor), varying with location. Comparisons between the DGPDF and (32 species) DSA results showed generally very good and at most conditions excellent, agreement [7].

2.1 Gas phase equations

The equation of state

$$p = (\rho R_u T)/m = cR_u T \quad (3)$$

is combined with Eulerian conservation equations for continuity, momentum, energy, species and first four moments $(\theta_v, \psi_v, \xi_{3v}, \xi_{4v})$ of the composition DGPDF, succinctly written as

$$\partial\Phi/\partial t + \partial[\Phi u_j]/\partial x_j = S + \partial[\Psi(\Phi)]/\partial x_j \quad (4)$$

where

$$\begin{aligned}\Phi &= \{c, cmu_i, cme_t, cX_v, \\ &\quad cX_v\theta_v, cX_v\psi_v, cX_v\xi_{3v}, cX_v\xi_{4v}\}\end{aligned} \quad (5)$$

$$\begin{aligned}S &= \{S_{\text{mole}}, S_{\text{mom},j}, S_{\text{en}}, \\ &\quad S_{\text{mole}}, S_{\text{mass}}, S_\psi, S_{\xi_3}, S_{\xi_4}\}\end{aligned} \quad (6)$$

$$
\begin{aligned}
\Psi(\Phi) \;=\; & \{cm\mathcal{D}\frac{\partial}{\partial x_j}\left[\frac{X_v}{m}\left(1-\frac{\theta_v}{m_a}\right)\right], \\
& p\delta_{ij}-\tau_{ij}, \\
& -u_i\tau_{ij}-\lambda\frac{\partial T}{\partial x_j}+\sum_{\zeta=1}^{N} J_{D\zeta,j}\left(h_\zeta-h_a\right), \\
& cm\mathcal{D}\frac{\partial}{\partial x_j}\left(\frac{X_v}{m}\right), cm\mathcal{D}\frac{\partial}{\partial x_j}\left(\frac{X_v\theta_v}{m}\right), \\
& cm\mathcal{D}\frac{\partial}{\partial x_j}\left(\frac{X_v\psi_v}{m}\right), cm\mathcal{D}\frac{\partial}{\partial x_j}\left(\frac{X_v\xi_{3v}}{m}\right), \\
& cm\mathcal{D}\frac{\partial}{\partial x_j}\left(\frac{X_v\xi_{4v}}{m}\right)\}
\end{aligned} \tag{7}
$$

where c is the molar density, x_i is the ith coordinate, $\mathbf{u}$ is the velocity, X is the mole fraction, $m=\theta_v X_v+m_a(1-X_v)$ is the molar mass where m_a is the carrier gas molar weight (subscript a denotes the carrier gas), $\mathcal{D}$ is an effective diffusion coefficient, p is the pressure, τ_{ij} is the viscous stress tensor, δ_{ij} is the Kronecker symbol, $e_t=e_k+e_{int}=u_iu_i/2+h-p/\rho$ is the total energy of the gas, $\rho=mc$ is the mass density, h is the enthalpy, λ is the thermal conductivity, T is the gas temperature and R_u is the universal gas constant. The last term in flux of the energy equation is the portion of the heat flux due to molar fluxes. The source terms, $S_{\text{mole}}, S_{\text{mom},j}, S_{\text{en}}, S_{\text{mass}}, S_\psi, S_{\xi_3}$ and S_{ξ_4} arise from the coupled interaction of drops and gas, and are given below.

2.2 Drop equations

All drops are individually simulated. Under the assumptions of quasi-steady gas phase with respect to the liquid phase (as $\rho/\rho_l=O(10^{-3})$ [19]) and of uniform internal drop properties (relatively small evaporation rate [18]; criterion checked *a posteriori*), the Lagrangian conservation equations for each drop position $\boldsymbol{\chi}$, velocity $\mathbf{v}$, energy, mass $M_d=\pi\rho_l D^3/6$ (subscript d denotes the drop) where D is the drop diameter, and composition are

$$
\frac{d\chi_i}{dt}=v_i, \quad \frac{dv_i}{dt}=\frac{F_i}{M_d} \tag{8}
$$

$$
\begin{aligned}
M_dC_{pl}\frac{dT_d}{dt} \;=\; & \underbrace{\frac{\lambda Nu}{D}\frac{\ln(1+B_T)}{B_T}A\left(T-T_d\right)}_{Q_{\text{conv-diff}}} \\
& \underbrace{+\dot{m}_d\frac{L_{veff}}{B}}_{Q_{\text{evap}}}
\end{aligned} \tag{9}
$$

$$
\dot{m}_d\equiv\frac{dM_d}{dt}=-\frac{Sh}{3\text{Sc}}\frac{M_d}{\tau_d}\frac{\ln(1+B)}{B} \tag{10}
$$

$$
\begin{aligned}
\frac{d\xi_{nl}}{dt} \;=\; & \frac{3\theta_l}{2BD^2}\frac{dD^2}{dt}\{[\frac{X_v}{m}-\frac{X_v^{(s)}}{m^{(s)}}(1+B)]\xi_{nl} \\
& +\frac{X_v^{(s)}\xi_{nv}^{(s)}}{m^{(s)}}(1+B)-\frac{X_v\xi_{nv}}{m}\}
\end{aligned} \tag{11}
$$

for $n\in[1,4]$, where the gas phase at the drop location, interpolated from the Eulerian solution, acts as the drop far field. $F_i=(M_d/\tau_d)f_1\left(u_i-v_i\right)$ where $\tau_d=\rho_lD^2/(18\mu)$ is the particle time constant for Stokes flow, T_d is the drop temperature, $A=\pi D^2$ is the drop-surface area and μ is the viscosity of the carrier gas; $\text{Pr}=\mu C_p/(\lambda m)$, where C_p is the heat capacity at constant pressure, and $Sc=\mu/(\rho\mathcal{D})$ are the Prandtl and the Schmidt numbers respectively. The Nusselt, Nu, and the Sherwood, Sh, numbers are semi-empirically modified using the Ranz-Marshall correlations, accounting for convective heat and mass transfer effects [14], with the similarity assumption $Nu=2+0.552\ \text{Re}_{sl}^{1/2}\left(\text{Pr}\right)^{1/3}, Sh=2+0.552\ \text{Re}_{sl}^{1/2}\left(Sc\right)^{1/3}$. f_1, given in [14], is an empirical correction to Stokes drag accounting for both finite droplet Reynolds numbers (slip Reynolds number $\text{Re}_{sl}=|\mathbf{u}-\mathbf{v}|\,\rho D/\mu$ where $(\mathbf{u}-\mathbf{v})$ is the slip velocity) and a Reynolds number based on the evaporation-due blowing velocity. $B=(Y_v^{(s)}-Y_v)/(1-Y_v^{(s)})$ is the Spalding number, where $Y_v=X_v\theta_v/m$ is the vapor mass fraction and $(1+B_T)=(1+B)^{1/Le}$ with Le being the Lewis number, L_{veff} is the effective latent heat [7] and the superscript (s) denotes the drop surface. At this surface, the classical drop boundary conditions of temperature equality, and mass, species, momentum and energy flux conservation [19] apply and Raoult's law relates (ideal-mixture assumed) the drop and gas PDFs

$$
P_v^{(s)}=\frac{p_{atm}}{X_v^{(s)}p}\exp\left[\frac{mL_v(m)}{R_uT_b(m)}\left(1-\frac{T_b(m)}{T_d}\right)\right]P_l^{(s)}. \tag{12}
$$

where $L_v(m)$ and $T_b(m)$ are the latent heat and the normal boiling point correlated as functions of m [7], and $p_{atm}=1atm$.

2.3 Source terms

The source-term-vector components of eq. 6 are

$$
S_r=-\sum_{q=1}^{N}\frac{w_q}{\Delta V_q}[\Lambda_r]_q \tag{13}
$$

$$
\begin{aligned}
\Lambda \;=\; & \{\frac{d\mathcal{N}}{dt}, F_j+\frac{d(\mathcal{N}\theta_l)}{dt}v_j, v_jF_j+Q_{\text{conv-diff}} \\
& +Q_{\text{evap}}+\frac{dM_d}{dt}\left(\frac{v_jv_j}{2}+C_{pl}T_d\right), \frac{d}{dt}(\mathcal{N}\theta_l), \\
& \frac{d(\mathcal{N}\psi_l)}{dt}, \frac{d(\mathcal{N}\xi_{3l})}{dt}, \frac{d(\mathcal{N}\xi_{4l})}{dt}\}
\end{aligned} \tag{14}
$$

where $\mathcal{N}_d=M_d/\theta_l$ is the number of moles in the drop, N is the number of drops, and the summation is over all drops residing within a local numerical discretization volume, ΔV_q. Following SC methodology [14], a geometric weighting factor w_q distributes the individual drop contributions to the nearest eight grid points in proportion to their distance from the

drop location; because convective effects dominate the species flux term, for MC flows, differential species diffusivity is negligible in transport from the drop location to the grid nodes.

3 Results

3.1 Configuration

Displayed in Fig. 1 is the mixing layer configuration showing the streamwise, x_1, cross-stream, x_2, and spanwise, x_3, coordinates with lengths $L_1 = 4\lambda_1 = 29.16\delta_{\omega,0}$, $L_2 = 1.1L_1$, and $L_3 = 4\lambda_3 = 0.6L_1$, with $L_1 = 0.2m$, where λ_1 and λ_3 are forcing wavelengths in the x_1 and x_3 directions, and are used to excite the layer in order to induce roll-up and pairing [20] [14], [21]. $\delta_{\omega,0} = \Delta U_0 / < \partial u_1/\partial x_2 >$ is the initial vorticity thickness (subscript 0 denotes the initial condition) where $\Delta U_0 = 2U_0$ is the velocity difference across the layer, the brackets $< >$ indicate averaging over homogeneous (x_1, x_3) planes, and the initial condition for u_1 is detailed in [14]; the initial mean streamwise velocity has an error-function profile [14]. The drops are randomly distributed throughout $x_2 < 0$ with uniform number density and uniform temperature $T_{d0} < T_0$, where T_0 is the initial uniform gas temperature; thus drop heating and evaporation ensues. The mean drop number density profile is smoothed near the center-line, $x_2 = 0$, using an error function profile. Table 1 summarizes the initial conditions. The initial drop slip velocity with respect to the gas is null, and the initial drop-size distribution is polydisperse and specified by the Stokes number, $St = \tau_d \Delta U_0/\delta_{\omega,0}$. Comparing MC and SC fuel parameters, it is obvious that one cannot have the same ρ_l, $< D_0 >$ and St_0. Because of the larger ρ_l at same initial St, the MC calculations are initialized with a larger number of drops, N_0, and a smaller $< D_0 >$ than their SC counterpart. Having the same St_0 in all computations means that if differences in the flow evolution occur, they are entirely the result of the SC versus MC aspect. The MC fuels considered are diesel [7] and three kerosenes (Jet A, RP1 and JP7) whose composition [24] was provided by Edwards [25]; all P_{l0} are SGPDFs, shown in Fig. 2 (mean and variance in Table 1). The PDF of the SC fuel (not shown) used for comparison, n-decane, is simply a delta function at $m = 142$kg/kmol. All thermodynamic properties were calculated as in Harstad et al. [7]. The mass loading, ML, is defined as the total mass of the liquid relative to the total mass of the gas in the laden stream.

Initially, the gas phase consists of carrier gas with a trace of vapor. The free-stream velocity $U_0 = M_{c,0} a_{C,0}$ is calculated from a specified value of the convective Mach number $M_{c,0}$ based on the carrier gas initial speed of sound. The specified value of the initial Reynolds number, $\mathrm{Re}_0 = \rho_0 \Delta U_0 \delta_{\omega,0}/\mu$, where ρ_0 is the initial gas density, is used to calculate μ. The thermal conductivity and diffusivity are then computed using this value of μ and (constant) specified values of $\mathrm{Pr} = Sc$, computed as in [26]. For each MC fuel, the initial vapor composition is found from a single-drop simulation is air at the specified T_0 by choosing it to be the first-time-step surface-vapor composition. To isolate the effect of the MC DGPDF representation, all thermophysical properties are those employed in the simulations of [21] [15] using air as the carrier gas and n-decane as the drop liquid.

The boundary conditions in the x_1 and x_3 directions are periodic and adiabatic slip-wall conditions in the x_2 direction previously derived [22] [23] were here adapted to the DGPDF CT model for MC mixtures. Drops reaching the slip walls are assumed to stick to them.

The equations were solved using the numerics detailed in [14] with the grid listed in Table 1. A fourth-order Lagrange interpolation procedure was used to obtain gas-phase variable values at drop locations. The drops whose mass decreased below 3% were removed from the calculation. The perturbations used to excite the layer are described elsewhere [14] [20].

3.2 Global layer evolution

The layer growth, measured by the momentum thickness [14], peaking at $t^* \equiv t\Delta U_0/\delta_{\omega,0} = 95$, is independent of the drop composition (not shown). The product thickness, defined in [14] measuring the global mixing, and plotted in Fig. 3, demonstrates substantial variability with the fuel. For $T_0 = 375$K, n-decane displays the best global mixing, generally followed by Jet A, RP1, JP7 and diesel. Differences between the simulations occur early in the layer evolution, and this high δ_P sensitivity may therefore constitute a good experimental diagnostic for comparing fuels. The early higher δ_P for Jet A compared to n-decane results from the initially higher evaporation rate of the former, as species more volatile than n-decane egress the drops. The final ordering of δ_P values is entirely correlated with the fuel saturation curve; this saturation curve is fixed for n-decane but is continuously evolving with time for MC fuels due to the change in composition. N-decane simulations at $T_0 = 400$K led to a substantial number of drops being evaporated before the second pairing, owing to the single value of $T_b = 447.7$K close to T_0, and thus the results were not conducive to studying drop-flow interactions. The MC-fuel formulation allows studies of the drop-flow interaction in the new regime of higher T_0. As expected, δ_P increases with T_0, as can be seen for diesel for $T_0 = 375\mathrm{K}, 400\mathrm{K}$ and 425K.

3.3 Drop composition

Shown in Fig. 4a and 4b for MC fuels is the liquid composition evolution in terms of $\{\theta_l\}/\theta_{l0}$ and $\{\sigma\}/\sigma_{l0}$, where $\{\}$ is the drop ensemble average. The initial $\{\theta_l\}/\theta_{l0}$ surge is accompa-

nied by a drastic reduction in $\{\sigma_l\}/\sigma_{l0}$ as the volatiles evaporate, and $\{\sigma_l\}/\sigma_{l0}$ reaches a minimum. This minimum, beyond which $\{\sigma_l\}/\sigma_{l0}$ continuously increases, coincides with a tapering off in the $\{\theta_l\}/\theta_{l0}$ increase. Therefore, both evaporation and condensation occur: condensation increases $\{\sigma_l\}/\sigma_{l0}$ whereas evaporation of the lightest species increases $\{\theta_l\}/\theta_{l0}$. Condensation is confirmed by plots of $\{B\}$ versus t^* (not shown) displaying some negative values.

Presented in Fig. 5 is $\{T_d/T_{sat}\}$ versus t^*, where T_{sat} is the fuel saturation temperature which for MC fuels is a function of composition. In all cases, a very mild $\{T_d/T_{sat}\}$ undulatory behavior is observed, traced to $\{T_d\}$ (not shown) manifesting evaporative cooling and heating cycles; ensemble averages conditioned on drop location (mixing layer for $x_2/\delta_{\omega,0} \geq -7$; complement is the lower stream) show this behavior to be biased by the larger number of drops in $x_2/\delta_{\omega,0} < -7$, as the mixing layer $\{T_d\}$ continuously increases after the first pairing. The variation of $\{T_d/T_{sat}\}$ for n-decane duplicates the behavior $\{T_d\}$ as T_{sat} is constant. For the MC fuels, the behavior is due to either the counteracting or concerting effect of T_d and T_{sat}. As the volatiles preferentially leave the drops, $\{T_{sat}\}$ increases concomitantly with $\{\theta_l\}/\theta_{l0}$ (not shown). At $T_0 = 375$K, the initial reduction of $\{T_d/T_{sat}\}$ combines the decrease in T_d with the increase in T_{sat}. At $T_0 > 375$K, two initial behaviors are seen: a reduction in $\{T_d/T_{sat}\}$ (diesel and Jet A) meaning that the increase in T_{sat} due to the evaporation of lower-m species is larger than the increase in T_d due to drop heating, or an augmentation in $\{T_d/T_{sat}\}$ (PR1 and JP7) meaning the opposite. The peaks and troughs in $\{T_d/T_{sat}\}$ emulate those of $\{T_d\}$ indicating that away from the initial condition, the global T_d variation is larger than that of T_{sat}.

3.4 Vapor composition

For a SC fuel the fuel vapor distribution is given by X_v. For MC fuels both the composition and X_v determine the species distribution. Displayed in Fig. 6a to 6b are the between-the-braid plane θ_v and σ_v shown as an example for MCdie375 at $t^* = 95$; the wide distribution of species is evident. The θ_v distribution shows that the lower stream is composed of mostly small-m species because they egress the drops first, before the drops are entrained into the mixing layer. Medium-m species are found in the mixing layer, as they evaporate after the light species and when the drops are already entrained. As the liquid composition changes to contain increasingly large-m species, the structure of the flow changes, with the establishment of regions of high drop number density profiling regions of high vorticity [27] [14]. The heaviest molar weight species reside at the location of the largest drop number density (not shown) because they are the last to evaporate, after the flow structure has been established. The upper stream still contains the initial vapor composition, as species have not been transported outside the ultimate vortex. Thus, a composition stratification is established, much as had been observed for laminar flow combustion with two species, where the simulations were performed with computational instead of physical drops [28]. Information not available in such binary-fuel computations is presented by σ_v which exhibits strong local variations, the smaller ones being in the lower stream, and the largest in the regions of highest θ_v. With increasing T_0, the upper range of both θ_v and σ_v increase (not shown), indicating that increasingly higher-m species are evaporated due to the increased T_d/T_{sat}, and also that the heterogeneity of the mixture increases. Homogeneous-plane averages of θ_v/θ_{v0} and σ_v/σ_{v0} displayed in Fig. 7a and 7b show the fuel-specific variations, although for all fuels the vapor is contained within the mixing layer and the lower stream; the lower stream uniform $< \theta_v > /\theta_{v0}$ and $< \sigma_v > /\sigma_{v0}$ is consistent with the saturation discussed above. Diesel evaporation produces the largest change in $< \theta_v > /\theta_{v0}$, mainly due to its very wide distribution (Fig. 2). The $< \theta_v > /\theta_{v0}$ peak coincides with the contour-plot-identified regions of high θ_v; this coincidence is even more pronounced for $< \sigma_v > /\sigma_{v0}$ showing first increased heterogeneity with the cross-stream distance, then the reaching of the above-discussed peak, and finally the decay to unity in the upper stream. Similar effects are exhibited by all kerosenes, with the difference that they are much less sensitive to T_0 and that the variations in the cross-stream direction are greatly reduced, both of which are attributed to their narrower initial PDF. At same T_0, the highest $< \theta_v > /\theta_{v0}$ is for diesel, and then in decreasing order for Jet A, JP7 and RP1, decreasing with the reduction in their initial PDF width. Of all kerosenes, Jet A produces the largest $< \theta_v > /\theta_{v0}$ in the mixing layer, consistent with the wider PDF on the high-m side, but relatively smaller values in the lower stream, consistent with the wider PDF on the low-m side. Similarly, the Jet A $< \sigma_v > /\sigma_{v0}$ displays more variation across the layer than the other kerosenes, which is again representative of its wider PDF. Thus, the composition of the gas phase mixture, which is responsible for ignition, combustion and pollutant production is highly variable with the MC fuel and must be captured if accurate predictions from combustion models are desired.

4 Conclusions

A formulation for describing the composition of MC fuels using a statistical representation has been used to derive a model of many drops evaporating in a flow. This model has been applied to study the evaporation of drops in a

three-dimensional temporal mixing layer whose lower stream is initially laden with a collection of randomly distributed polydiperse drops. The layer initially contains four spanwise vortices whose double pairing, promoted by a perturbation, results in the formation of an ultimate vortex. The results are analyzed to study the layer and drop evolution as well as the state at the highest momentum thickness of the layer. Comparisons are made among simulations performed with a SC fuel (n-decane), diesel and three kerosenes: Jet A, RP1 and JP7. The results show substantial differences between the global and local mixing features of the layers, all of which are traced to the relative initial composition of the fuels. Strong composition nonuniformities in the layer, found for all MC fuels, means that SC fuels cannot capture the necessary species distribution to model combustion. Moreover, the species distribution is fuel-specific, offering the possibility to discriminate between fuel-composition-related combustion efficiency, pollutant formation, corrosion aspects, etc. The simulations show that the identified composition effects are amplified with increasing temperature. Likewise, for Reynolds numbers larger than that of the simulations, evaporation will be enhanced resulting again in amplified composition heterogeneity. Thus, turbulent combustion models must realistically include fuel composition effects.

Acknowledgements

This study was conducted at the Jet Propulsion Laboratory (JPL), California Institute of Technology (Caltech), under the partial sponsorship of the Donors of The Petroleum Research Fund administered by the American Chemical Society through a grant (to JB) for Caltech Post Doctoral Fellow support, the U.S. Department of Energy with Ms. R. Danz and Mr. D. Hooker as contract monitors, under an agreement with the National Aeronautics and Space Administration, and the Air Force Research Laboratory, Wright Patterson Air Force Base with Dr. J. T. Edwards as Technical Monitor. Additional sponsorship was provided by the Office National d'Études et de Recherches Aérospatiales for Post Doctoral support. We wish to thank Dr. K. G. Harstad for helpful discussions. Computational resources were provided by the supercomputing facility at JPL.

References

[1] C. K. Law and H. K. Law, *AIAA J.* 20 (1982) 522–527.

[2] C. M. Megaridis and W. A. Sirignano, *Proc. Comb. Inst.* 23 (1990) 1413-1421.

[3] K. Harstad and J. Bellan, *Atomization and Sprays* 1 (1991) 367–388.

[4] J. Tamim and W. L. H. Hallett, *Chem. Eng. Sci.* 50 (1995) 2933-2942.

[5] W. L. H. Hallett, *Combust. Flame* 121 (2000) 334-344.

[6] A. M. Lippert and R. D. Reitz, SAE paper 97FL-468, 1997.

[7] K. G. Harstad, P. C. Le Clercq and J. Bellan, *AIAA J.*, 41(10) (2003) 1858-1874.

[8] B. Gal-Or, H. T. Cullinan, Jr. and R. Galli, *Chem. Eng. Sci.* 30 (1975) 1085-1092.

[9] R. L. Cotterman, R. Bender and J. M. Prausnitz, *Ind. Eng. Chem. Process Des. Dev.* 24 (1985) 194–203.

[10] C. H. Whitson, *Soc. Pet. Eng. J.* 23 (1983) 683-694.

[11] M. T. Rätzsch, and H. Kehlen, *Fluid Phase Equilibria* 14 (1983) 225-234.

[12] G. F. Chou and J. M. Prausnitz, *Fluid Phase Equilibria* 30 (1986) 75-82.

[13] K. G. Harstad and J. Bellan, paper F9, Western States Meeting of the Combustion Institute, October 2003, Los Angeles, CA; submitted 2003.

[14] R. S. Miller and J. Bellan, *J. Fluid Mech.* 384 (1999) 293-338.

[15] N. Okong'o and J. Bellan, Consistent Large Eddy Simulation of a temporal mixing layer laden with evaporating drops. Part I: Direct Numerical Simulation, formulation and *a priori* analysis, accepted in *J. Fluid Mech.*, 2003

[16] M. Boivin, S. Simonin and K. D. Squires, *J. Fluid Mech.* 375 (1988) 235-263.

[17] F. Mashayek, *J. Fluid Mech.* 367 (1998) 163–203.

[18] A. Makino and C. K. Law, *Combust. Flame* 73 (1988) 331-336.

[19] F. A. Williams, *Combustion Theory*, Addison-Wesley, 1965

[20] R. D. Moser and M. M. Rogers, *Phys. Fluids A*, **3** (1991) 1128–1134.

[21] R. S. Miller and J. Bellan, *Phys. Fluids* 12(3) (2000) 650-671.

[22] T. J. Poinsot and S. K. Lele, *J. Comp. Phys.* 101 (1992) 104–129.

[23] M. Baum, T. J. Poinsot and S. K. Lele, *J. Comp. Phys.* 116 (1994) 247-261.

[24] T. Edwards, L. Q. Maurice, *J. Propul. Power* 17(2) (2001) 461-466.

[25] T. Edwards, private comm. (2002).

[26] R. S. Miller, K. Harstad and J. Bellan, *Int. J. Multiphase Flow* 24 (1998) 1025-1055.

[27] K. D. Squires and J. K. Eaton, *Phys. Fluids* A 3 (1991) 1169-1178.

[28] G. Continillo and W. A. Sirignano, *Proc. Comb. Inst.* 22 (1988) 1941-1949.

Figure captions

Figure 1. Mixing layer configuration.

Figure 2. Liquid initial PDF for each fuel.

Figure 3. Timewise evolution of the product thickness. (— —) SCdec375, (—) MCdie375, (–□–) MCdie400, (–▽–) MCdie425, (- - -) MCjetA375, (-□-) MCjetA400, (-··-) MCrp1375, (-⊡-) MCrp1400, (-···-) MCjp7375, (-··⊡-) MCjp7400.

Figure 4. Timewise evolution of the normalized ensemble average liquid a) mean molar weight and b) standard deviation. Legend in Fig. 3.

Figure 5. Timewise evolution of the ensemble average liquid drop temperature normalized by the saturation temperature. Legend in Fig. 3.

Figure 6. Contour plots of the a) mean molar weight and the b) standard deviation in the between-the-braid plane $x_3/\delta_{\omega,0} = 8.75$ at $t^* = 95$ for MCdie375.

Figure 7. Homogeneous-plane average of the normalized vapor a) mean molar weight and b) standard deviation. Legend in Fig. 3.

Case	fuel	T_0	ρ_{l0}	$\{\{D_0\}\}(\times 10^{-4})$	θ_{l0} / σ_{l0}	θ_{v0} / σ_{v0}	$N_0(\times 10^3)$
SCdec375	n−decane	375	642	1.365	142 / NA	142 / NA	580
MCdie375	diesel	375	828	1.202	185.0 / 43.0	140.0 / 28.0	670
MCdie400	diesel	400	828	1.164	185.0 / 43.0	140.0 / 28.0	690
MCdie425	diesel	425	828	1.129	185.0 / 43.0	140.0 / 28.0	720
MCjetA375	Jet A	375	800	1.223	161.0 / 29.7	140.0 / 23.5	675
MCjetA400	Jet A	400	800	1.184	161.0 / 29.7	140.0 /23.5	695
MCrp1375	RP1	375	800	1.223	165.2 / 17.7	153.5 / 14.8	675
MCrp1400	RP1	400	800	1.184	165.2 / 17.7	153.5 / 14.8	695
MCjp7375	JP7	375	800	1.223	167.1 / 19.2	153.7 / 15.7	675
MCjp7400	JP7	400	800	1.184	167.1 / 19.2	153.7 / 15.7	695

Table 1: Initial conditions. T_0 in degrees K, ρ_{l0} in kg/m^3, D_0 in m and mean molar weights and standard deviations in kg/kmol. In all simulations, $M_{c,0}$=0.4, $\delta_{\omega,0}$=6.859×10^{-3}m, $\{\{St_0\}\}$=3 and $\{\{(St_0 - \{\{St_0\}\})^2\}\}^{1/2}$=0.5, $\mathrm{Re}_0 = 200$, $ML_0 = 0.2$, $X_{v0} = 10^{-4}$, T_{d0}=345K, γ=86kg/kmol for diesel, γ=41kg/kmol for Jet A, and γ=93kg/kmol for RP1 and JP7, the grid=200×224×120, and CPU time $\simeq$ 792 hours on a SGI Origin 2000 and 274 hours on a cluster with Intel Itenium2 processors.

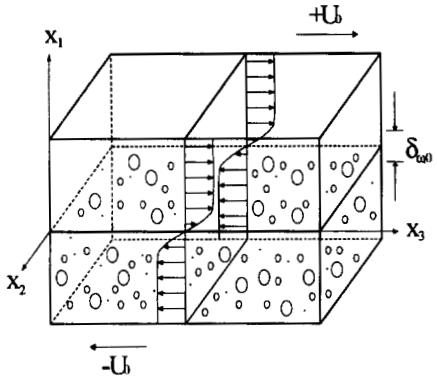

Figure 1: Mixing layer configuration.

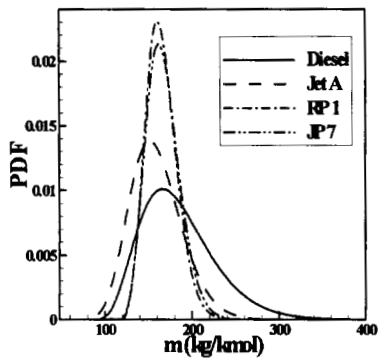

Figure 2: Liquid initial PDF for each fuel.

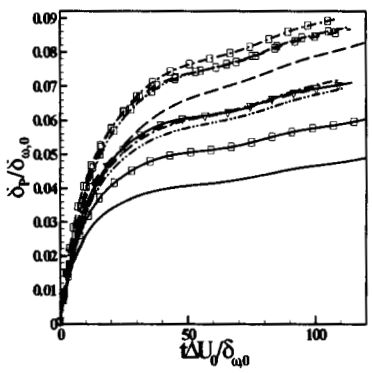

Figure 3: Timewise evolution of the product thickness. (— —) SCdec375, (—) MCdie375, (-□-) MCdie400, (-▽-) MCdie425, (- - -) MCjetA375, (-□-) MCjetA400, (-··-) MCrp1375, (-⊡-) MCrp1400, (-···-) MCjp7375, (-·⊡-) MCjp7400.

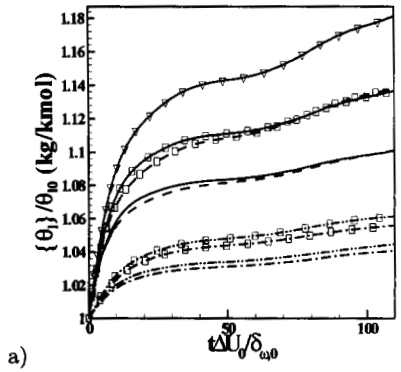

a)

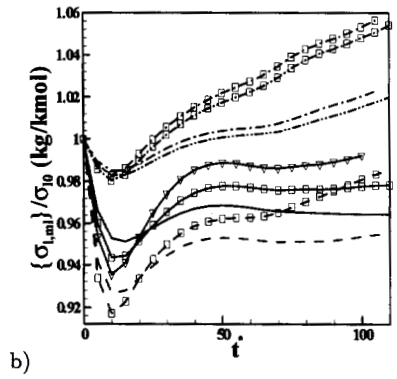

b)

Figure 4: Timewise evolution of the normalized ensemble average liquid a) mean molar weight and b) standard deviation. Legend in Fig. 3.

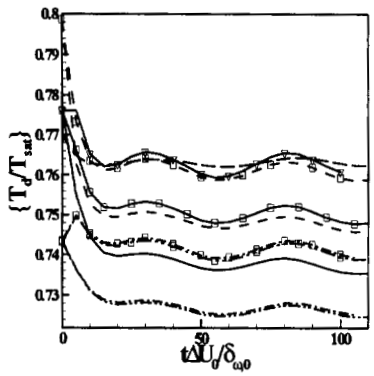

Figure 5: Timewise evolution of the ensemble average liquid drop temperature normalized by the saturation temperature. Legend in Fig. 3.

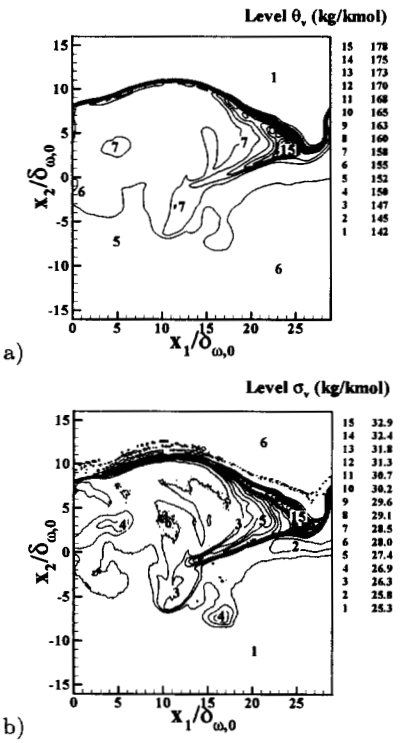

Figure 6: Contour plots of the a) mean molar weight and the b) standard deviation in the between-the-braid plane $x_3/\delta_{\omega,0} = 8.75$ at $t^* = 95$ for MCdie375.

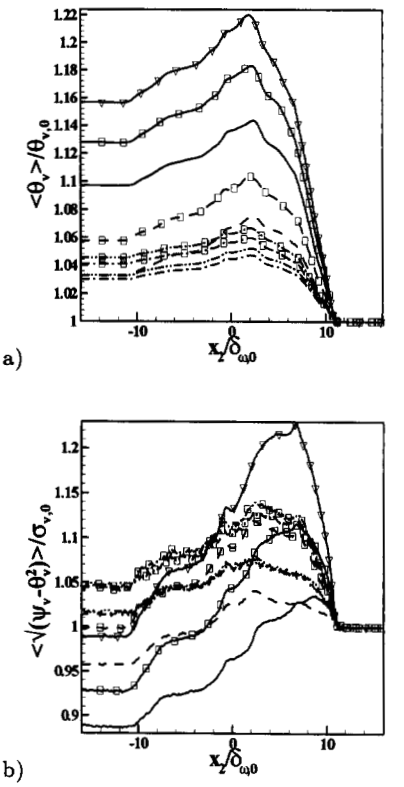

Figure 7: Homogeneous-plane average of the normalized vapor a) mean molar weight and b) standard deviation. Legend in Fig. 3.